Pressure dependence of the magic twist angle in graphene superlattices

Stephen Carr, Shiang Fang, Pablo Jarillo-Herrero, and Efthimios Kaxiras

Pressure dependence of the magic twist angle in graphene superlattices

Stephen Carr,[1] Shiang Fang,[1] Pablo Jarillo-Herrero,[2] and Efthimios Kaxiras[1]

[1]Department of Physics, Harvard University, Cambridge, Massachusetts 02138, USA.
[2]Department of Physics, Massachusetts Institute of Technology, Cambridge, MA, USA.
(Dated: August 9, 2018)

The recently demonstrated unconventional superconductivity[1] in twisted bilayer graphene (tBLG) opens the possibility for interesting applications of two-dimensional layers that involve correlated electron states. Here we explore the possibility of modifying electronic correlations by the application of uniaxial pressure on the weakly interacting layers, which results in increased interlayer coupling and a modification of the magic angle value and associated density of states. Our findings are based on first-principles calculations that accurately describe the height-dependent interlayer coupling through the combined use of Density Functional Theory and Maximally localized Wannier functions. We obtain the relationship between twist angle and external pressure for the magic angle flat bands of tBLG. This may provide a convenient method to tune electron correlations by controlling the length scale of the superlattice.

I. INTRODUCTION

Recent experimental results in twisted bilayer graphene (tBLG) have shown it to be an important system for understanding unconventional superconductivity,[1] and more generally correlated physics in two-dimensional (2D) materials.[2] This discovery comes after systematic development of experimental techniques which at present allow for twist angle control in stacked 2D heterostructures with a remarkable precision of $0.1°$.[3–6] In bilayer graphene, a relative twist between the layers by a "magic" angle produces just the right amount of band hybridization to form flat bands near the Fermi level.[7–15] The flat bands have the majority of their electron density located at the AA-stacking regions of the moiré supercell. As the Fermi velocity goes to zero, the scale of the electron kinetic energy falls below the scale of the two-particle Coulomb interaction, producing correlated behavior, although the precise mechanism for these effects is still a topic of active research (see Refs. [16–19] for a non-exhaustive list). Understanding the nature of the flat bands induced by the magic angle twist in tBLG is vital in studies of correlated electrons in 2D, and could lead to the discovery of other systems with similar behavior, generally referred to as "twistronics".[20] We present here an ab-initio study of how the interlayer electronic coupling in tBLG depends on external uniaxial pressure in the direction perpendicular to the layers, and how pressure acts as an additional tuning parameter for creating flat bands in magic angle tBLG and its associated correlated physics.

Manipulating superconductivity in tBLG by external pressure would follow the historic trend of using pressure to probe the nature of the superconducting T_c.[21,22] The T_c in conventional BCS superconductors usually decreases with pressure, but in unconventional superconductors pressure often increases T_c. This is attributed to strong dependence of electronic correlation on external pressure, although the exact mechanism is not well un-
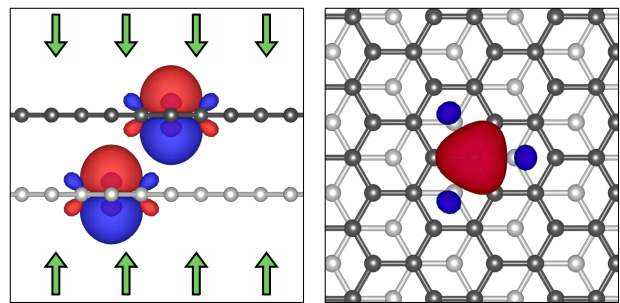

FIG. 1. Isosurfaces of the localized Wannier functions in bilayer graphene, with the colors indicating different signs. (Left) Side view: Vertical compression of the bilayer mainly causes the orbitals to overlap more, thus increasing interlayer coupling while leaving in-plane couplings mostly unaffected. (Right) Top view: The triangular shape and nodes (indicated by the sign change) introduce angular dependence effects in the interlayer coupling, neglected in empirical tight-binding models for bilayer graphene based on p_z orbitals.

derstood and may vary between materials. 2D materials are particularly sensitive to pressure along the direction perpendicular to the layers, as they are coupled through weak van der Waals interactions. The mechanical effects of pressure on monolayer graphene have been documented through a variety of methods,[23–25] and recently electronic transport measurements were performed on a graphene-hBN device under pressure.[26]

II. METHODS

In previous work we have derived ab-initio tight binding hamiltonians for a range of 2D materials, including graphene, by using the maximally localized Wannier orbitals[27] to represent first-principles calculations based on density functional theory (DFT).[28,29] Our model for bilayer graphene identified a strong angular dependence of the interlayer coupling between the Wannier orbitals

(see Fig. 1). The tight binding parameters are obtained by first using a conventional DFT code (we use VASP[30]) to find the electronic-ground state Kohn-Sham wavefunctions in a standard plane-wave basis, $\psi_i(k)$, and then transforming these into a localized real-space basis, $\phi_i(r)$. After the transformation, the DFT hamiltonian can be used to compute the energy overlap matrix elements $\langle \phi_i | H | \phi_j \rangle = t_{ij}$, which give the hopping parameters of a tight-binding model. A 4-band tight-binding model of bilayer graphene was determined, consisting of intralayer hopping energies and a functional form for interlayer coupling. This interlayer coupling function included angular dependence due to the triangular warping of the p_z type orbitals of carbon in the simplified graphene model. It is given as a sum of three terms, representing the different angular momenta of the wavefunctions:

$$t(\mathbf{r}) = V_0(r) + V_3(r)[\cos(3\theta_{12}) + \cos(3\theta_{21})] \\ + V_6(r)[\cos(6\theta_{12}) + \cos(6\theta_{21})] \tag{1}$$

with the radial functions given by

$$V_0(r) = \lambda_0 e^{-\xi_0(\bar{r})^2} \cos(\kappa_0 \bar{r})$$
$$V_3(r) = \lambda_3 \bar{r}^2 e^{-\xi_3(\bar{r}-x_3)^2} \tag{2}$$
$$V_6(r) = \lambda_6 e^{-\xi_6(\bar{r}-x_6)^2} \sin(\kappa_6 \bar{r})$$

where $\bar{r}$ is $r/2.46\text{Å}$, the in-plane radius reduced by the in-plane lattice parameter. This form takes into account both the in-plane radius and the relative angles between the displacement vector and the monolayer lattices.

To extend the model to compressed tBLG, we performed additional DFT calculations[30] to derive the relationship between external uniaxial pressure and interlayer distance in the bilayer as well as the pressure-dependent parameterization of the tight-binding hamiltonian. Compression of the bilayer is given throughout the work in terms of $\epsilon = 1 - (d/d_0)$ where d is the local interlayer distance and d_0 is the distance at zero external pressure ($d_0 = 3.35$ Å from our calculations). Although in a free-floating bilayer system the lattice parameters are likely to change under compression, most experimental studies create these devices by encapsulating them in insulating substrates, usually hBN. This encapsulation technique may change the in-plane lattice parameter as well, and so for simplicity we have ignored these effects. To compare the compression parameter ϵ to an experimental pressure of an encapsulated system, we have also calculated the external pressure of a bulk system consisting of three 2D layers: AB bilayer graphene separated by a single layer of hBN. We approximate the lattice-paramter of hBN as equal to that of graphene, 2.46 Å, meaning the system consists of only six atoms, 2 from each layer. Energies are computed in the VASP DFT software package with the van der Waals DFT method

i (y_i)	$c_i^{(0)}$	$c_i^{(1)}$	$c_i^{(2)}$
1 (λ_0)	0.310	-1.882	7.741
2 (ξ_0)	1.750	-1.618	1.848
3 (κ_0)	1.990	1.007	2.427
4 (λ_3)	-0.068	0.399	-1.739
5 (ξ_3)	3.286	-0.914	12.011
6 (x_3)	0.500	0.322	0.908
7 (λ_6)	-0.008	0.046	-0.183
8 (ξ_6)	2.272	-0.721	-4.414
9 (x_6)	1.217	0.027	-0.658
10 (κ_6)	1.562	-0.371	-0.134

TABLE I. Fitted compression dependence for the 10 parameters of the interlayer coupling model. All parameters are given in units of eV and take the form given in Eq. 4.

SCAN+rVV10 of Peng et al.,[31] a k-mesh of $21 \times 21 \times 1$, and an energy cutoff of 500 eV. We simulate pressure by changing the height of the periodic cell and allow the graphene atoms to fully relax, but fix the locations of the hBN atoms. No significant restructuring of the graphene bilayer due to compression was observed. The pressure from the DFT calculations is well fit by the functional form

$$P = A\left(e^{-B\epsilon} - 1\right) \tag{3}$$

with $A = 5.73$ GPa and $B = 9.54$, displayed in Fig. 2.

We find that vertical compression of the bilayer has negligible effect on the in-plane tight-binding parameters, but significantly strengthens interlayer coupling. The pressure dependence of the 10 parameters of the interlayer coupling function[29] are well described by a quadratic fit

$$y_i(\epsilon) = c_i^{(0)} + c_i^{(1)}\epsilon + c_i^{(2)}\epsilon^2 \tag{4}$$

where y_i, $i = 1, \ldots, 10$ represents one of the 10 parameters of the model. The fitted values for each of the 10 parameters is given in Table I.

The three λ_n parameters ($n = 0, 3, 6$) have the strongest dependence on ϵ, while every other parameter is only weakly dependent. This makes sense, as the λ_n's set the overall strength of the electronic coupling between the layers and should increase quickly as the layers are forced closer together. The other parameters encode angular and radial-centering information of the interlayer coupling, and are thus less affected by compression. The robust compression dependence of the parameters λ_n is shown in the inset of Fig. 2, where $n = 0, 3, 6$ corresponds to the three lowest channels of orbital angular momentum.
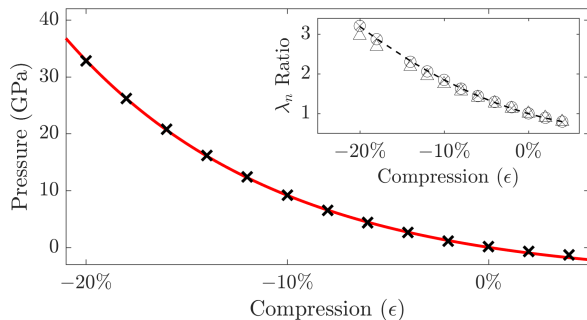
FIG. 2. Calculated vertical external pressure as a function of interlayer distance between graphene layers (black crosses) with the the fit given in the text (red line). Inset: Compression dependence of the primary scaling parameters λ_n of the interlayer coupling formula normalized by their values at $\epsilon = 0$. Values for $n = 0, 3, 6$ are shown with crosses, circles, and triangles respectively. The quadratic fit for λ_0 is given by the dashed line.

III. RESULTS

A. Pressure dependence of the magic angle

In Fig. 3(a) we show the low energy electronic structure of tBLG at three different twist angles and compressions, calculated with a supercell tight-binding model. The magic angle can be thought of as a resonance of the bilayer hybridization, where the twist angle acts as a "knob" tuning the electronic structure.[20] As the compression increases and the layers come closer to one another the effective interlayer coupling strength increases, causing stronger electronic hybridization between them. In particular, while the zero-pressure magic angle occurs at approximately $1.1°$, under 10% compression (9.2 GPa) the magic angle is approximately $2.0°$. Our calculations did not show significant reconstruction of the graphene bilayer under pressure even up to 30 GPa, but there may be a phase transition of the encapsulating hBN substrate around 9 GPa.[26]

A heuristic argument for tracking the magic angle as a function of compression or twist angle can be constructed from the perspective of coupled states in momentum space, as shown in Fig. 3(b). Without interlayer coupling, the low-energy band structure of a bilayer resembles two Dirac cones separated in momentum space by $K_\theta \approx G\theta$, where G is the characteristic length of the reciprocal-cell lattice vectors of the monolayer. For simplicity, we avoid the complexities of scattering in momentum space that the twist angle introduces, and focus on the Bloch states which are exactly halfway between the K and K' points of the supercell (the M point). Before hybridization, each layer contributes two Bloch states with energies $\pm(K_\theta/2)\hbar v_F$, where v_F is the Fermi velocity of a graphene monolayer. We expect eigenvalues near 0 when the interlayer coupling terms are equal in magnitude to the Bloch state energies. A derivation including nearest-

neighbor momentum scattering can give a more precise relationship for these terms,[9] but for our argument this is not necessary as we will only be interested in the relative scaling of inter and intralayer energies. We then assume this interlayer coupling strength t has at most quadratic dependence on compression,

$$t(\epsilon) = t_2\epsilon^2 - t_1\epsilon + t_0 \propto \hbar v_F \frac{K_\theta}{2}. \qquad (5)$$

Taking into account that $K_\theta \propto \theta$ and that there is a magic angle at zero compression ($\epsilon = 0$) of approximately $\theta_0 = 1.12°$, we can make the substitution $\hbar v_F(K_\theta/2) \rightarrow \theta(t_0/\theta_0)$ to obtain:

$$t_2\epsilon^2 - t_1\epsilon + t_0(1 - \theta/\theta_0) = 0 \qquad (6)$$

which gives the critical value, $\theta_c(\epsilon)$, of the magic angle as a function of compression ϵ:

$$\theta_c(\epsilon) = \theta_0 \left[(t_2/t_0)\epsilon^2 - (t_1/t_0)\epsilon + 1 \right]. \qquad (7)$$

From this expression, we deduce that for experimentally accessible pressures any angle in the range $[1.1°, 3.0°]$ can serve as the magic twist angle that leads to correlated behavior, by adjusting the pressure.

To confirm this claim, we use an *ab-initio* $k \cdot p$ model, as described in a previous work,[32] to sample the electronic bandstructure of tBLG under compression and with a twist angle in the estimated range. This approach is an exact Bloch basis expansion of a tight binding hamiltonian. It differs from empirical $k \cdot p$ models[9] in the accuracy of the interlayer coupling matrices (often named T_i). These simplified models assume the coefficients of T_i are momentum independent, whereas the *ab-initio* approach introduces T_i dependence on the overall momentum of the relevant Bloch states. A complete Fourier transform of the spatially dependent interlayer coupling, sampled on a fine mesh, is used to calculate band structure without the commensurate angle restriction. The method is primarily limited by the sampling of the interlayer coupling form, especially near the magic angle. This is controlled by ensuring the bands near the Fermi level are converged within a few meV of conventional supercell results at a few selected commensurate angles. We assume the twisted bilayer has its origin of rotation though a pair of stacked orbitals at AA stacking (D_3 symmetry), but the results here would not change if one considers the axis of rotation through the lattices' hexagon center instead (D_6 symmetry).

To quantify the "flatness" of the band-structure we compute the bandwidth of the two bands closest to the Fermi level at the Γ point (Brillouin zone center). As seen in Fig. 3(a), the bandwidth of the low-energy states at this point is on the order of a few meV, which gives a reliable indication of how flat the bands are. In Fig. 3(c) we show the bandwidth at the Γ point, referred to here as
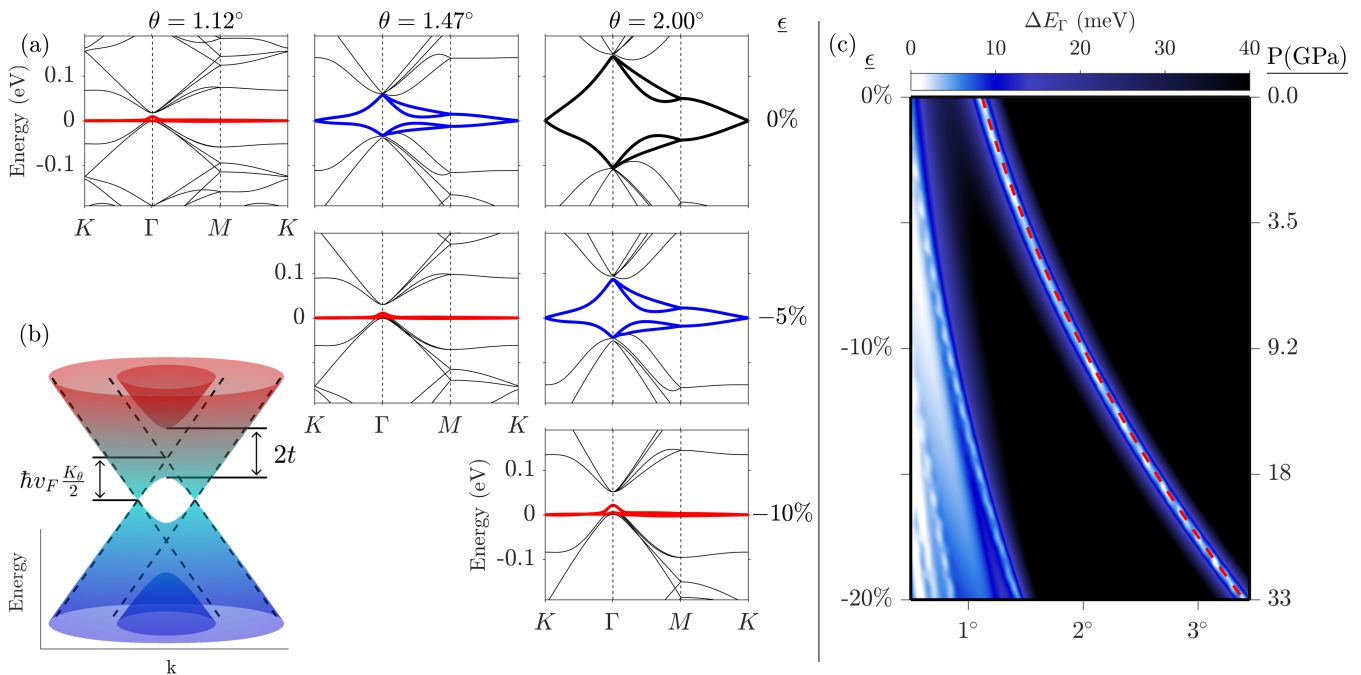
FIG. 3. **(a)** Band structures for twisted bilayer graphene under compression ϵ from the *ab initio* tight-binding model. The flat-band regime is achieved at 5% compression for a twist angle of $1.47°$, and at 10% compression for a twist angle of $2.00°$. **(b)** The two coupled Dirac cones, shifted in momentum space due to the twist, and with interlayer coupling strength λ_0, are shown schematically. **(c)** Critical values of the compression parameter ϵ as a function of twist angle calculed by an *ab-initio* $k \cdot p$ model. The bandwidth of the eight bands closest to the Fermi level at the Γ point, ΔE_Γ, is shown in color with white representing the small bandwidth of the flat bands. The dashed red line gives the expected value of the compression to cause flat bands (see text for details).

ΔE_Γ, as a function of twist angle and compression. The most prominent feature (white line) corresponds to the first magic angle value. The lines at smaller angles correspond to higher-order magic angles. The relationship derived from our heuristic argument agrees extremely well with numerical results if we use the values of the leading scaling parameter of the interlayer coupling, λ_0, and reduce the linear and quadratic terms by 8%. Additional parameters for the interlayer coupling beyond λ_0 are required to describe the pressure effects accurately, such as the angular distribution and range of the coupling. Their inclusion in the model would affect the interlayer coupling in $k \cdot p$ theory, leading to this small correction. The corrected values are $t_{[0,1,2]} = [0.310, 1.731, 7.122]$ eV.

B. Relaxation Effects

As a final ingredient to enhance the reliability of the theoretical model, we use the distance dependent interlayer coupling to examine the effects of atomic relaxation in tBLG systems at 0 pressure. The uncompressed bilayer exhibits significant relaxation at a twist angle of approximately $1°$.[6,13,33–35] This causes important changes to the low-energy bandstructure,[36] and in the $k \cdot p$ formalism can be understood as breaking the symmetry between the AA and AB interlayer coupling coefficients as the AA (AB) regions are greatly reduced (increased) in size.[18] Just as compression enhances electronic coupling between the layers, it also enhances atomistic coupling. At large compression, significant relaxation is likely to occur at larger angles, including those that lead to flat bands under external pressure.

In Fig. 4 we present our *ab-initio* tight-binding band-structure results for tBLG with and without relaxation. The relaxation is taken into account by using a continuum model that uses only DFT values from generalized stacking fault calculations[37] adapted for twisted systems.[38] This model relaxes both the in-plane and the out-of-plane positions of the atoms and updates the interlayer coupling accordingly, but currently cannot include pressure. Under external pressure, the relaxation model will need to include local changes to both the elastic energy of the individual graphene layers, and the sensitive height dependence of the interlayer stacking energy. Since we have found that relaxation does not significantly alter the value of the magic angle in the zero pressure case, the expected magic angles calculated above are unlikely to be greatly changed by pressure-dependent relaxation effects.

Although the magic angle is roughly the same when relaxation is considered, the structure of the flat bands and the size of the single-particle gaps change with the re-
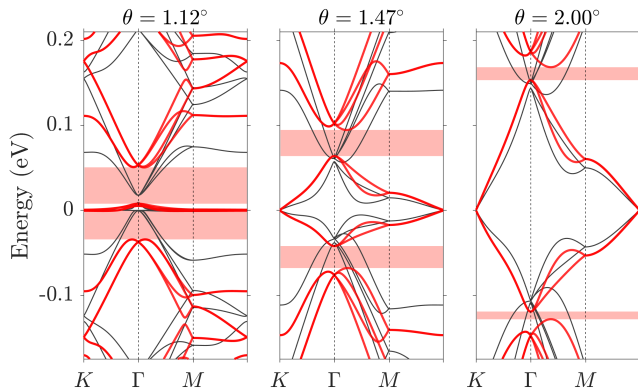
FIG. 4. Band structures of uncompressed twisted bilayer graphene with and without relaxation of the atoms. The black lines are bands for the unrelaxed system and the red lines for the relaxed system. The single particle gaps in the relaxed system are highlighted in pink.

laxation correction. This also indicates that experimental study of correlation effects can depend sensitively on the sample's environment and substrate effects. We find that relaxation increases the dispersion of the low energy bands and increases the gaps on both sides to roughly 50 meV near the magic angle, which is in good agreement with experiment.[2,3] At larger angles the relaxation is less extreme, and the gap size decreases with increasing angle. Near 2° the gaps are almost completely gone as the unrelaxed and relaxed bilayer geometry become similar. Quantifying the degree of relaxation in experimental devices will be an important ingredient for understanding the low energy electronic structure, and thus the superconductivity phenomenon, in graphene.

IV. CONCLUSION

We have studied the behavior of flat bands induced by magic angle twist in bilayer graphene as a function of external pressure. The height dependent coupling allows for accurate band structure calculation for relaxed systems, showing that relaxation can play an important role in interpreting the low energy states of twisted bilayer graphene. We demonstrated how the pressure may be used to produce correlated behavior, identified by the presence of flat bands at twist angles that increase with increasing pressure. Although the correlation mechanism remains uncertain, the larger twist angles lead to a moiré cell of smaller size, which is likely beneficial to the coupling strength and may enhance correlated electron behavior, including the superconducting T_c. In the absence of clear understanding of the superconducting state it is impossible to provide *quantitative* predictions for these effects. Inverting the argument, we propose that systematic experimental study of correlated behavior as a function of pressure could shed light on the nature of unconventional superconductivity in tBLG and related systems.

[1] Y. Cao, V. Fatemi, S. Fang, K. Watanabe, T. Taniguchi, E. Kaxiras, and P. Jarillo-Herrero, Nature **556**, 43 EP (2018), article.

[2] Y. Cao, V. Fatemi, A. Demir, S. Fang, S. L. Tomarken, J. Y. Luo, J. D. Sanchez-Yamagishi, K. Watanabe, T. Taniguchi, E. Kaxiras, R. C. Ashoori, and P. Jarillo-Herrero, Nature **556**, 80 EP (2018).

[3] Y. Cao, J. Y. Luo, V. Fatemi, S. Fang, J. D. Sanchez-Yamagishi, K. Watanabe, T. Taniguchi, E. Kaxiras, and P. Jarillo-Herrero, Physical Review Letters **117**, 116804 (2016).

[4] K. Kim, M. Yankowitz, B. Fallahazad, S. Kang, H. C. P. Movva, S. Huang, S. Larentis, C. M. Corbet, T. Taniguchi, K. Watanabe, S. K. Banerjee, B. J. LeRoy, and E. Tutuc, Nano Letters **16**, 1989 (2016), pMID: 26859527, http://dx.doi.org/10.1021/acs.nanolett.5b05263.

[5] K. Kim, A. DaSilva, S. Huang, B. Fallahazad, S. Larentis, T. Taniguchi, K. Watanabe, B. J. LeRoy, A. H. MacDonald, and E. Tutuc, Proceedings of the National Academy of Sciences **114**, 3364 (2017), http://www.pnas.org/content/114/13/3364.full.pdf.

[6] H. Yoo, K. Zhang, R. Engelke, P. Cazeaux, S. H. Sung, R. Hovden, A. W. Tsen, T. Taniguchi, K. Watanabe, G.-C. Yi, M. Kim, M. Luskin, E. B. Tadmor, and P. Kim, preprint (2018).

[7] G. Li, A. Luican, J. M. B. Lopes dos Santos, A. H. Castro Neto, A. Reina, J. Kong, and E. Y. Andrei, Nature Physics **6**, 109 (2009).

[8] E. Suárez Morell, J. D. Correa, P. Vargas, M. Pacheco, and Z. Barticevic, Phys. Rev. B **82**, 121407 (2010).

[9] R. Bistritzer and A. H. MacDonald, Proceedings of the National Academy of Sciences of the United States of America **108**, 12233 (2011).

[10] A. Luican, G. Li, A. Reina, J. Kong, R. R. Nair, K. S. Novoselov, A. K. Geim, and E. Y. Andrei, Phys. Rev. Lett. **106**, 126802 (2011).

[11] P. San-Jose, J. González, and F. Guinea, Physical review letters **108**, 216802 (2012).

[12] I. Brihuega, P. Mallet, H. González-Herrero, G. Trambly de Laissardière, M. M. Ugeda, L. Magaud, J. M. Gómez-

Rodríguez, F. Ynduráin, and J.-Y. Veuillen, Physical review letters **109**, 196802 (2012).

[13] K. Uchida, S. Furuya, J.-I. Iwata, and A. Oshiyama, Physical Review B **90**, 155451 (2014).

[14] D. Wong, Y. Wang, J. Jung, S. Pezzini, A. M. DaSilva, H.-Z. Tsai, H. S. Jung, R. Khajeh, Y. Kim, J. Lee, S. Kahn, S. Tollabimazraehno, H. Rasool, K. Watanabe, T. Taniguchi, A. Zettl, S. Adam, A. H. MacDonald, and M. F. Crommie, Physical Review B **92**, 155409 (2015).

[15] H. Nishi, Y.-i. Matsushita, and A. Oshiyama, Phys. Rev. B **95**, 085420 (2017).

[16] H. C. Po, L. Zou, A. Vishwanath, and T. Senthil, preprint (2018).

[17] N. F. Q. Yuan and L. Fu, Phys. Rev. B **98**, 045103 (2018).

[18] M. Koshino, N. F. Q. Yuan, T. Koretsune, M. Ochi, K. Kuroki, and L. Fu, preprint (2018).

[19] J. F. Dodaro, S. A. Kivelson, Y. Schattner, and C. W. Xiao-Qi Sun, preprint (2018).

[20] S. Carr, D. Massatt, S. Fang, P. Cazeaux, M. Luskin, and E. Kaxiras, Phys. Rev. B **95**, 075420 (2017).

[21] C. Chu and B. Lorenz, in *Frontiers in Superconducting Materials*, edited by A. V. Narlikar (Springer, Berlin, 2005) pp. 459–497.

[22] C. Chu and B. Lorenz, Physica C: Superconductivity **469**, 385 (2009), superconductivity in Iron-Pnictides.

[23] J. E. Proctor, E. Gregoryanz, K. S. Novoselov, M. Lotya, J. N. Coleman, and M. P. Halsall, Phys. Rev. B **80**, 073408 (2009).

[24] J. Nicolle, D. Machon, P. Poncharal, O. Pierre-Louis, and A. San-Miguel, Nano Letters **11**, 3564 (2011), pMID: 21805986, https://doi.org/10.1021/nl201243c.

[25] M. Yankowitz, K. Watanabe, T. Taniguchi, P. San-Jose, and B. J. LeRoy, Nature Communications **7**, 13168 EP (2016), article.

[26] M. Yankowitz, J. Jung, E. Laksono, N. Leconte, B. L. Chittari, K. Watanabe, T. Taniguchi, S. Adam, D. Graf, and C. R. Dean, Nature **557**, 404 (2018).

[27] N. Marzari, A. A. Mostofi, J. R. Yates, I. Souza, and D. Vanderbilt, Rev. Mod. Phys. **84**, 1419 (2012).

[28] S. Fang, R. Kuate Defo, S. N. Shirodkar, S. Lieu, G. A. Tritsaris, and E. Kaxiras, Physical Review B **92**, 205108 (2015).

[29] S. Fang and E. Kaxiras, Physical Review B **93**, 235153 (2016).

[30] G. Kresse and J. Furthmller, Computational Materials Science **6**, 15 (1996).

[31] H. Peng, Z.-H. Yang, J. P. Perdew, and J. Sun, Phys. Rev. X **6**, 041005 (2016).

[32] D. Massatt, S. Carr, M. Luskin, and C. Ortner, Multiscale Modeling & Simulation **16**, 429 (2018), https://doi.org/10.1137/17M1141035.

[33] M. M. van Wijk, A. Schuring, M. I. Katsnelson, and A. Fasolino, 2D Materials **2**, 034010 (2015).

[34] S. Dai, Y. Xiang, and D. J. Srolovitz, Nano Letters **16**, 5923 (2016), pMID: 27533089, http://dx.doi.org/10.1021/acs.nanolett.6b02870.

[35] K. Zhang and E. B. Tadmor, Journal of the Mechanics and Physics of Solids **112**, 225 (2018).

[36] N. N. T. Nam and M. Koshino, Phys. Rev. B **96**, 075311 (2017).

[37] S. Zhou, J. Han, S. Dai, J. Sun, and D. J. Srolovitz, Phys. Rev. B **92**, 155438 (2015).

[38] S. Carr, D. Massatt, S. B. Torrisi, P. Cazeaux, M. Luskin, and E. Kaxiras, preprint (2018).